Leiden University

Exoplanets A: Interiors and Atmospheres

Ultra-Hot Rocky Planets (Lava Worlds)

Authors:
Claire Olde Loohuis (s3313980)
Catherine Slaughter (s3238865)
Louis Siebenaler (s3211126)
Benjamin Silk (s1850237)
Yuze Zhang (s2819368)

July 10, 2023

1 Introduction

Ultra-hot rocky planets, or *lava worlds*, are a class of rocky (exo)planets characterized by the presence of volcanic activity and 'magma oceans' due to extreme surface temperatures. Magma oceans can form on rocky planets with short orbital periods due to strong radiation from their host star.

The molten surfaces, atmospheres of vaporized rock, and the interactions between the two provide an opportunity to probe the interior composition of lava worlds, and by extension rocky planets, through observations of their atmospheres (e.g. Kite et al. 2016). Moreover, lava worlds could also provide a glimpse into the early history of the Earth and other terrestrial planets in the Solar system, since lava worlds are theorized to also be a stage in the formation and evolution of rocky planets, even without small orbital radii (Elkins-Tanton 2012).

The extreme nature of lava worlds therefore makes them unique laboratories in space for studying the formation, evolution, both interior and atmospheric compositions, and potential habitability of rocky planets.

This report begins in the interior of lava worlds and works its way outward. In Section 2, the mechanisms governing heating and transport in the interiors of lava worlds are described, as well as the magma oceans and their evolution over time. In Section 3, the structure, composition (including chemistry), and behavior of the atmospheres of lava worlds are explained. The link between the atmosphere, surface, and interior of lava worlds is also described. Sections 2 and 3 are also accompanied by descriptions of studies modelling lava world interiors and atmospheres. Finally, in Section 4, a brief overview of lava world observations is given, and an example of a well-studied lava world, K2-141b, is described.

2 Interiors and Evolution

Our understanding of the interiors of lava worlds and the evolution of their magma oceans is mainly based on studies of planets in our solar system and lava lakes found on Earth. In this section, we will first introduce the main energy sources which power sustained activity on lava worlds, followed by interior models and the evolution of magma oceans.

2.1 Sources of Heat

In general, three energy sources work together to maintain a magma ocean. These include radionuclides, insolation and tidal heating.

The decay of short-lived radionuclides, unstable isotopes with mean lifetimes between 10^3 and 10^6 yrs, is thought to have been the principal internal heat source of planets in the early solar system. The most important radionuclide is ^{26}Al, based on the high fraction of ^{26}Mg (daughter isotope of ^{26}Al) in primitive meteorites found on Earth (Dauphas & Chaussidon 2011). If exoplanets form closer to the center of the galaxy, near a recent supernova or neutron star merger, the abundance of radionuclides can be much higher, thus promoting the presence of lava worlds. Furthermore, most lava world candidates are akin to super-Earths, given their increased mantle mass and hence higher abundance of radiogenic material, capable of fueling intense volcanic activity by a lower surface-to-volume ratio (Henning et al. 2018).

Insolation can set extremely high surface temperature conditions (1500–3000 K) which surpass the melting point of many mineral species in the mantle region. Hence, depending on the

planet's proximity to its host star, insolation may facilitate and sustain a lava world without excess internal heat provided by radionuclides.

For eccentric orbits or non-synchronous rotation, the planet experiences tidal deformation which induces tidal heating in the interior (Driscoll & Barnes 2015). The exact upper limits of this heating mechanism are uncertain as it depends on a number of properties. Firstly, tidal dissipation circularizes the planetary orbit and thus decreases with time, unless the eccentricity is maintained by a perturbing planet or stellar companion (Chao et al. 2021). Moreover, tidal heating depends on mantle rheology and decreases as the the interior temperature approaches the solidus (Driscoll & Barnes 2015).

It is worth emphasizing that there exist other sources of energy, such as giant gravitational energy, giant impacts, and internal induction, which contribute to the formation of magma oceans, however they do not ensure the sustained volcanic activity on lava worlds.

2.2 Interiors of Lava Worlds

The planetary structure of lava worlds is generally believed to consist of a rocky interior with possible melt in both the mantle and core. The core is assumed to be dominated by Fe and FeS. However, with increasing data precision due to ongoing missions like CHEPOS, the addition of light metals such as S, Si, O, C, and Ni (Valencia et al. 2007) may become important. Most models assume an adiabatic core thermal profile, with a temperature jump at the core-mantle boundary due to residual heat released during core formation, thus making the core hotter than the mantle (Dorn & Lichtenberg 2021). The mantle has a bulk silicate composition with the main density determining components corresponding to SiO_2, CaO, Al_2O_3, MgO, FeO(T)[1], Na_2O, and K_2O (Kite et al. 2016). Due to the extreme temperatures in lava worlds, part of the mantle will be molten, producing magma oceans. The depth of the magma ocean is set by a transition between a fluid-like and solid-like behavior at a critical crystal fraction. High pressure favors crystallization (Stevenson 2010), and so with depth the melt fraction drops and the crystallizing magma acquires strength through continuous crystal chains. At 40% melt fraction, 'lock-up' takes place which puts the remaining melt into isolated channels (Stevenson 2010), and the material is regarded as solid again due to a significant increase in viscosity. For tidally locked planets, without significant circulation within the magma ocean, the ocean depth can be estimated to be $\mathcal{O}(10$ km) (Kite et al. 2016).

Magma oceans are not calm: there is a constant magma flow driven by gradients in temperature, composition, and crystal fraction. At the same time, the magma experiences fractional evaporation due to its content of volatiles such as H_2O, CO_2 and SO_2. Surface composition for magma oceans is set by the competition between the magma flow, which refreshes the surface with the bulk material of the magma ocean on a timescale τ_T, and evaporation, which produces a chemically varied surface on a timescale τ_X (Kite et al. 2016). Hence, when $\tau_X/\tau_T \ll 1$, chemical differentiation between the magma ocean surface layer and interior may occur. In this scenario, the atmosphere will not sample the bulk composition of the pool. On the other hand, when $\tau_X/\tau_T \gg 1$, the magma ocean can evolve into a well-mixed entity and the atmosphere will effectively probe the magma ocean.

[1]FeO(T) stands for FeO, Fe_2O_3, Fe_3O_4, or a mixture depending on the oxidation state.

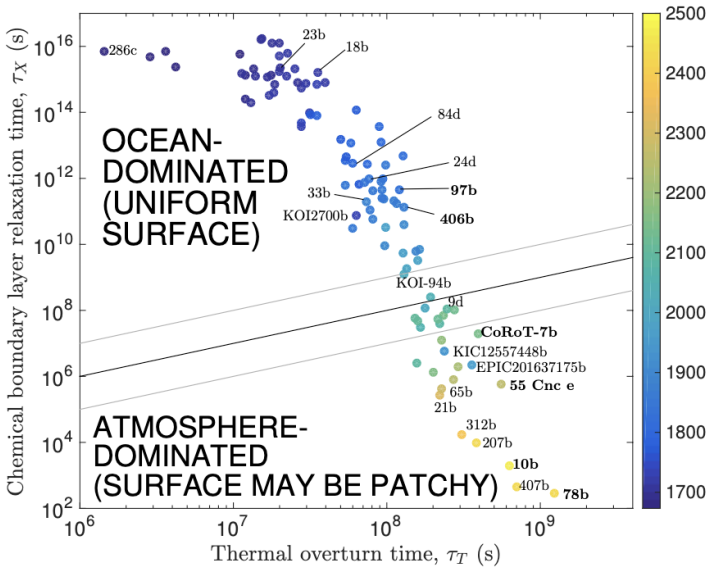

Figure 1: Figure from Kite et al. (2016), showing the ocean-overturn timescale τ_T vs the surface fractionation timescale τ_X. The datapoints are colored according to the magma ocean surface temperature. The results are obtained using a 1D atmospheric model and assume fractional vaporization of 20% of fractionating volume and rocky planets with radius $R = 0.3$ R_{Earth} and mass $M \approx 0.01$ M_{Earth}. Labelled datapoints correspond to true exoplanets, whose known properties were used to estimate τ_T and τ_X. The black line corresponds to $\tau_X = \tau_T$.

2.3 Evolution of Magma Oceans

As described in Section 2.2, competition between evaporation and circulation determines the magma ocean's surface composition. Figure 1 (Kite et al. 2016) shows the timescales τ_T and τ_X as a function of surface temperature. This reflects that homogeneous oceans are obtained at lower temperatures, since circulation defeats evaporation, whereas hotter magma oceans may have compositionally varied surfaces which take the form of stratified residual magma. The stability of the stratified layers depends on the density contrast between the fractionated reservoir and bulk material of the magma ocean. Kite et al. (2016) investigated the evolution and stability of magma-oceans using the `MAGMA` melt-vapor equilibrium code (Fegley & Cameron 1987, Schaefer & Fegley 2004) for fractional evaporation of melt at 2000 K for a range of bulk silicate (mantle + crust) compositions. `MAGMA` computes the chemical equilibria in the melt, between the melt and its equilibrium vapor, and in the gas phase. They find that a high concentration of Fe-oxide in the planet's silicate mantle favors stable stratification of the residual magma. Fe-oxide rich magma oceans are characterized by high bulk densities $\rho_0 > 3000$ kg/m^3, and upon fractional vaporization, the density of the fractionated reservoir never exceeds ρ_0. This produces a boundary layer which stays buoyant (i.e stable stratified layers develop) and re-equilibration with the deep interior of the magma ocean is inhibited. Hence, in this case a compositionally evolved surface is expected to form on the lava world on a timescale $\tau_X \ll 1$ Gyr (see Figure 1), which strongly depends on the mean evaporation rate within the magma ocean. On the other hand, if the planetesimals that formed the planet have Earth-like bulk silicate compositions (i.e poor in Fe-oxide), the density of the magma oceans will be significantly lower: $\rho_0 \sim 2700$ kg/m^3. As a result, fractionally evaporated residual melt exceeds the initial density ρ_0 once it becomes CaO-rich (at ~ 81 wt% fractional vaporization), and the boundary layer sinks into the underlying magma. This process repeatedly resets the surface composition to the planet-averaged silicate composition.

3 Atmospheres: Composition, Structure, and Behavior

3.1 The Dual Atmosphere

Atmospheres of lava worlds can be diverse, and are distinct from other planetary atmospheres due to their strong dependence on the composition of the magma ocean and the complex feedback loops which can result (Chao et al. 2021). Theoretically, it is possible for a magma ocean to exist on a planet with a thick, CO_2–H_2O dominated atmosphere as long as it is able to retain its volatiles. However, due to the short-period, close-in predilection of lava worlds, stellar irradiation and/or lack of volatiles more commonly lead to a thin silicate-vapor atmosphere (Chao et al. 2021). The expectation of tidal locking for short-period planets further reduces this atmosphere, relegating it to the day side and resulting in a hemispherical magma ocean (Boukaré et al. 2022).

3.2 Atmospheric Heat Transfer

In the silicate-vapor atmosphere considered here, the surface temperature of the planet can be well approximated by local radiative equilibrium; the atmosphere is so optically thin that the effects of convection are trivial and, in the vertical direction, heat is transported via radiative transfer (Boukaré et al. 2022, Zilinskas et al. 2022). Heat can also be exchanged horizontally in the atmosphere via supersonic winds. The transfer of heat and mass from the day side to the airless night side occurs rapidly, and is driven by the relationship between pressure and local surface temperature. If the atmospheric scale height H is small compared to planet radius, pressure gradients (and, where rotational forces are eclipsed by inertial forces, winds) are directed away from the high-temperature substellar point and towards the low-temperature night side (Kite et al. 2016). After evaporation, the acquired mass is either lost to space or condensed into clouds and deposited outside of the magma ocean (Kite et al. 2016). The heat is swiftly dissipated, as the temperature contrast between day and night sides can exceed 2000 K (Boukaré et al. 2022). It should be noted, however, that Castan & Menou (2011) find that this atmospheric heat flux is small compared to insolation for surface temperatures $\ll 3500$ K, and that the surface energy budget is dominated by radiative flux, making understanding the atmospheric thermal structure crucial.

3.3 Thermal Structure of the Atmosphere

In an attempt to shed light on the observability of existing lava worlds, and to further scrutinize findings of atmospheric temperature inversion in Ito et al. (2015), Zilinskas et al. (2022) modelled thin silicate atmospheres via the computation of temperature-pressure profiles and emission spectra. To achieve this, the outgassed chemistry of the atmosphere was modelled using the `MAGMA` code (see Section 2.3) and the `FASTCHEM` thermochemical equilibrium code (Stock et al. 2018). The main adopted melt composition was that of the Bulk Silicate Earth (BSE), though other viable silicate compositions were considered. Details of all compositions can be viewed in Table 1 of Zilinskas et al. (2022), but for our purposes, these compositions are split into two groups: bulk melts (BSE, Komatiite, Mercury) which are dominated by SiO_2 and MgO, and crustal melts (Continental, Oceanic) dominated by SiO_2 and Al_2O_3.

Temperature structure for the BSE melt was ascertained by solving the two-stream approximation using the radiative transfer code `HELIOS` (Malik et al. 2017; 2019). No surface albedo

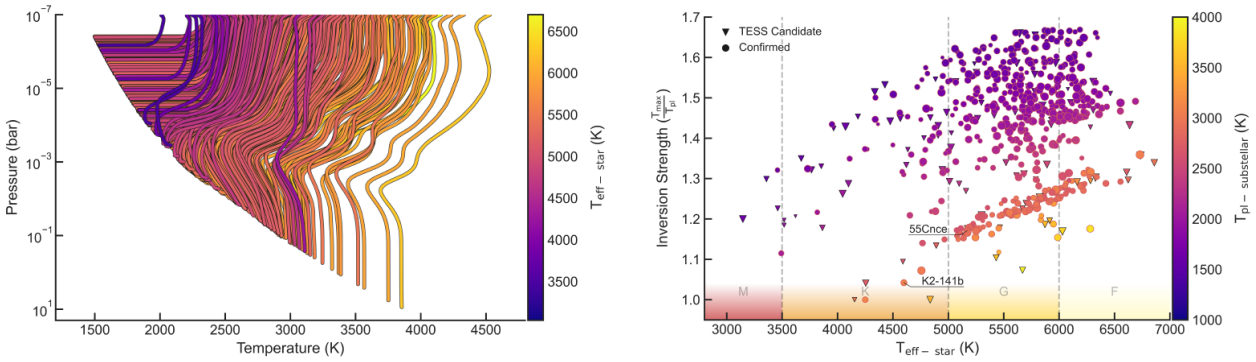

Figure 2: Plots from Zilinskas et al. (2022) displaying (left) the temperature-pressure profiles of confirmed lava planets with BSE compositions, where color indicates stellar irradiation temperature and (right) the strength of the thermal inversion of the atmosphere, where color indicates planetary temperature. Inversion strength is defined as the ratio of the maximum atmospheric temperature to planet's surface temperature; it scales linearly with stellar temperature, and is inversely related to planet temperature.

was assumed, and the profiles were converged to the radiative-convective equilibrium. It was found that thermal structure is highly dependent on surface temperature, and that inversion strength and surface temperature are inversely correlated: at temperatures around 1500 K, the profile is low-pressure ($\sim 10^{-7}$ bar), nearly isothermal, and sparse in complex molecules. As the temperature rises ($\sim$2000 K), pressure increases ($\sim 10^{-3}$ bar) enough to push the photosphere away from the surface and confine inversions to the upper portion of the atmosphere. Temperatures of $\sim$2500 K incur surface pressures of $\sim 10^{-2}$ bar and the creation of a tropopause below the inversion. Further increase in surface temperature ($\sim$4000 K) may cause the atmosphere to become unstable, rendering it completely opaque, trapping regions below the photosphere, and opening it up to erosive mass loss.

Additional effects in the temperature-pressure profile are caused by the nature of the irradiation from the host star. Due to hot star emission peaking at shorter wavelengths and cooler stars peaking in the IR, inversion strength scales linearly with host star temperature. Then atmospheres with the strongest thermal inversions will be found around hot G- and F-stars, while only mild inversions should be detected around M-type stars or K-dwarfs. The relation between thermal inversion strength, stellar temperature, and planetary temperature can be seen in Figure 2, accompanied by a depiction of the temperature-pressure profiles of confirmed lava planets.

Differences in composition between the bulk melt and crustal melt groups result in enhanced short wave absorption, so that stronger atmospheric temperature inversions occur in lava planets with a crustal melt structure.

3.4 Chemistry of the Atmosphere

Section 2.3 highlights how evaporation and circulation impact the magma ocean surface composition on some lava worlds. It is also important to highlight how such processes impact the atmospheric composition of these planets. Through outgassing processes, observations of hot rocky exoplanet atmospheres may provide unique insight into their interiors; insight which is not possible with other rocky planet types. As such, it is important to develop a theoretical understanding of the chemistry of these atmospheres. There are two crucial components to this: first, a clear relationship between planetary surface composition and atmospheric composition

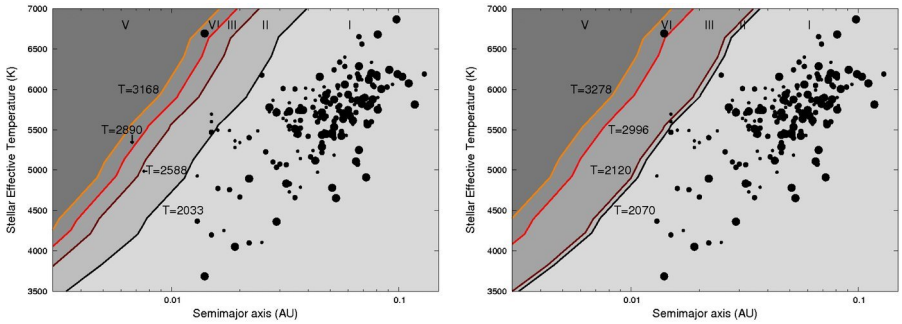

Figure 3: Figure from Miguel et al. (2011), showing the regions on a plot of semi-major axis vs. stellar effective temperature where each of the five atmosphere types is found for both a komatiite (left) and bulk silicate Earth (right) composition.

at equilibrium, and second, setting expectations for what spectral and phase curve observations of such atmospheres ought to look like, and assessing their observability.

3.4.1 Relationship Between Atmospheric and Surface Composition

Several past studies (Léger et al. 2011, Castan & Menou 2011, Kite et al. 2016) have attempted to ascertain atmospheric parameters for several individual observed ultra-hot rocky planets. These studies indicate agreement that such planets have semi-volatile atmospheres comprised primarily of silicates. There have also been studies (Schaefer & Fegley 2009, Miguel et al. 2011) which worked to create more generalised compositional results based specifically on outgassing models.

Miguel et al. (2011), in particular, compared a number of such models to ultra-short period rocky exoplanets from the 2011 *Kepler* data release (Borucki et al. 2011). The methods of this paper build off of Schaefer & Fegley (2004; 2009), and assume atmospheres in which volatile gasses such as H, C, N, and S have already escaped on short timescales, based on extensive observational evidence (Spencer & Schneider 1996, Baraffe et al. 2005, Leitzinger et al. 2011). Without this escape, such gasses would very quickly dominate the composition of their atmospheres (Schaefer et al. 2012). Miguel et al. (2011) created atmospheric models for planets with two distinct surface compositions, containing SiO_2, MgO, Al_2O_3, TiO_2, Fe_2O_3, FeO, CaO, Na_2O, and K_2O (See Miguel et al. (2011), Table 1). Using `MAGMA`, they created atmospheric models over a range of planetary and stellar parameters, based on those from the *Kepler* data. They found that, for a given magma composition, the relevant system parameters are those which impact planetary surface temperature, i.e. aspects such as planet mass are not consequential. In doing so, they identified five distinct atmosphere types, where the expected atmosphere composition (for a given magma composition) is dependent on planetary temperature (see Fig. 3). Each atmosphere type is characterized by its majority composition, as outlined in Table 1.

More recently, an updated code, `LavAtmos` (Van Buchem et al. 2022), has been developed to build off of and improve the results of `MAGMA`-based studies. `LavAtmos` works to calculate the equilibrium composition of the rock vapor for a given magma composition and temperature. This code takes into account nine different oxides (SiO_2, MgO, Al_2O_3, TiO_2, Fe_2O_3, FeO, CaO, Na_2O, and K_2O) and thirty-one vapor types (with corresponding reactions). As of the writing of this report, the paper outlining `LavAtmos` has been submitted for publication (Van Buchem et al. 2022), wherein the authors determine that the code's results correspond well with both

Type	Surface Temperature	Majority Composition
I	< 2033 K	Na, O_2, O, Fe
II	2033–2588 K	Na, O_2, O, SiO, Fe, Mg
III	2588–2890 K	Na, O_2, O, SiO, Mg, Fe
IV	2890–3168 K	Silicate- and Na-Dominated
V	> 3168 K	SiO, O, O_2, Na

Table 1: The surface temperatures and Majority Compositions for the five types of lava world atmospheres described in Miguel et al. (2011). The surface temperatures given correspond to an Earth-like komatiite surface composition. Note that the *Majority Composition* column is generally listed in order of highest to lowest column density.

published data from lab-based chemistry studies as well as other modelling codes. Future work making use of `LavAtmos` should be illuminating.

3.4.2 Potential Observability Modelling

Due to the particular connection between atmospheric and surface compositions on lava worlds, it is additionally important to understand how such processes may impact current and future observations of such planets. Several studies (Ito et al. 2015, Zilinskas et al. 2022; 2023), all of which make use of `MAGMA`, have attempted to model emission spectra using modelled atmospheres. All of these studies are in general agreement with Miguel et al. (2011), finding that such atmospheres are expected to be primarily composed of Na, K, Fe, Si, SiO, O, and O_2. Zilinskas et al. (2022; 2023) focus primarily on emission signals within the range of the MIRI instrument on JWST. In general, they find that SiO (and, less commonly) SiO_2 may serve as the most useful identifiers for this instrument. Additionally, Zilinskas et al. (2023) focus on atmospheres which are rich in lighter volatiles like H, C, and N (assumed to be younger atmospheres). They find that the observability of SiO is hindered by volatiles such as H_2O and H^-, and impacted by the C/O ratio in the atmosphere. They conclude that observed lava planets to have strong SiO emission are likely to have a high metallicity and low C/O (a possible indication of efficient transfer between the surface and atmosphere).

3.5 Atmospheric Evolution

As briefly discussed in Section 2.2, the evolutionary behavior of the magma ocean can affect the composition of the atmosphere: in planets with surface temperatures >2400 K, inhomogeneity of the melt can lead to fractional vaporization (Kite et al. 2016). Subsequently, and especially in planets which are strongly irradiated, the acquired volatiles are swiftly lost to space or transferred to the night side of the planet, where they condense out. In all cases of atmospheric evolution considered by Zilinskas et al. (2022), Na, the most volatile component, was rapidly lost, followed by the depletion of K, Fe, and Si. The effect on a planet with surface temperature larger than 2000 K is a drop in atmospheric pressure of $\mathcal{O}(10^2)$, a removal of shortwave opacity, and a weakening of thermal inversions. As more volatiles are removed, the photosphere and tropopause are displaced upward to lower pressures, and a greenhouse effect is induced which can raise the surface temperature by up to 200 K (Zilinskas et al. 2022). Moreover, removal of absorbers causes the spectral features of the atmosphere to diminish, making them more difficult to observe. This effect is felt most strongly by lava planets orbiting cooler stars; around hot stars the effect is similar, albeit less prominent.

4 Observing Lava Worlds

4.1 Detection Methods and Existing Surveys

The most successful and most widely employed method for lava planet detection is the transit method. The majority of exoplanets are discovered via transit photometry by *Kepler* and the Transiting Exoplanet Survey Satellite (TESS) (Koch et al. 2010, Ricker et al. 2014, Deeg & Alonso 2018). By using the transit method, one can detect ultra-short period planets (USPs) near G-type stars or stars with higher temperatures. Planets detected near M-type dwarf stars, however, might have a lower equilibrium temperature given their transit period, and are less likely to host magma oceans (Jehin et al. 2016, Dittmann et al. 2017). Hence, the classification of lava planets heavily depends on the host star's properties (Berger et al. 2020).

The Doppler radial velocity (RV) method is mostly used for planet mass determination and to validate planet candidates found by transit photometry. The RV-determined planet mass, on top of the transit-determined planet radius, yields the mean density of the observed planet, which can be compared to various models for planet interiors (Dorn et al. 2017, Lopez 2017). The planet's radius and mass can also be used for surface gravity calculation, which is important for modelling the planet's atmosphere (Ciardi et al. 2019). In addition, the RV helps to constrain the eccentricity of the planet's orbit, which provides information for tidal dissipation, a driver for melting on lava worlds (Driscoll & Barnes 2015).

Transit photometry in combination with transit spectroscopy can contribute to analysis of the structure and constituents of the planet's atmosphere (Kreidberg 2018). During transit, the apparent planet size might vary with respect to frequency. Mutli-wavelength observations, therefore, can provide the aforementioned information about the planet's atmosphere, especially sulphur compounds from volcanism on lava planets (Kaltenegger & Traub 2009). Unlike normal rocky Earth-like planets, the high surface temperature of lava worlds allows its temperature to be measured via the infrared emission during the secondary eclipse, and broad features from molecular absorption lines of this IR emission are helpful diagnostics of the planet's atmospheric composition (Garhart et al. 2020, MacDonald et al. 2020).

In the past, several attempts were made to measure the phase curves of lava planets on ∼1-day orbits (Batalha et al. 2011, Sanchis-Ojeda et al. 2013, Hu et al. 2015, Demory et al. 2016b, Angelo & Hu 2017). The change in flux from unresolved planets with phase offer insights into the scattering properties at the surface of the atmosphere. The longitudinal variation in atmospheric structure and temperature between the day and night side of the planet can also be analyzed thanks to infrared phase curves provided by *Spitzer* (Koll & Abbot 2015). Studied features include the shift of the planet's peak infrared emission or "hotspot" resulting from heat transport and thermal inertia of the atmosphere as well as longitudinal variation in albedo and cloud structures. These analyses are crucial for understanding the efficiency of heat transport of the planet's atmosphere, which might depend on the planet's rotation and atmospheric composition (Zhang & Showman 2017, Parmentier & Crossfield 2018, Rauscher et al. 2018).

Besides transit photometry in combination with previously mentioned methods, direct imaging is another detection technique for exoplanets, which spatially or spectrally separates the planet's signal from its host stars. However, direct imaging is currently limited to young supergiant planets with large orbital periods (Crossfield et al. 2015).

Method	Parameters	Notable Surveys/Missions
Transit Photometry	P, R_p	*CoRot*, *Kepler*, *TESS*
Doppler RV	P, $M_p \sin i$, e	HIRES, HARPS, ESPRESSO, EXPRES
Transmission Spectra	Atmosphere	*Hubble*, *Spitzer*, *JWST*
Secondary Eclipse	T_{eq}, A	*Kepler*, *Spitzer*, *JWST*
Phase Curves	Day/Nightside Variations	*Kepler*, *Spitzer*, *JWST*

Table 2: Exoplanet observation methods (From Chao et al. 2021).

4.2 An Example Lava World: K2-141b

One recent observation effort of a lava exoplanet is the *Spitzer* phase curve analysis of K2-141 b (Zieba et al. 2022). The target is a transiting USP rocky planet with a radius of 1.51 ± 0.05 $R_\oplus$ (similar to the majority of the observed USPs with $R_p < 2$ $R_\oplus$), which was discovered by the *Kepler* space telescope during its K2 mission and is orbiting a K-type dwarf star with an orbital period of 6.7 hours (Howell et al. 2014, Barragán et al. 2018, Malavolta et al. 2018). An observation of the star by the high-precision spectrograph HARPS-N results in a planet's mass of $M_p = 5.08 \pm 0.41$ $M_\oplus$. Provided the average density of the planet, $\rho = 8.2 \pm 1.1$ g/cm^3, the planet is expected to have an iron-silicate (Earth-like) composition.

Previously, an optical phase curve and a secondary eclipse with a depth of 23 ± 4 ppm were revealed by *Kepler*. The calculated equilibrium temperature of K2-141b is around 2150 K under full atmospheric heat redistribution and 2745 K in case of instant re-radiation (Koll et al. 2019). Like one of the best-studied small USP planets, 55 Cnc e, K2-141 b has the potential to become another ideal benchmark to compare to other USPs. The bright host star (V=11.5 mag, K=8.4 mag) also allows observations of the planet's emission in the infrared, and K2-141 b is one of the only two lava planets, besides 55 Cnc e, accessible in both the infrared and the optical regimes (Demory et al. 2016a;b). In fact, the two planets have similar profiles except for the inconsistency between their compositions (55 Cnc e is inconsistent with an Earth-like composition of 30% Fe).

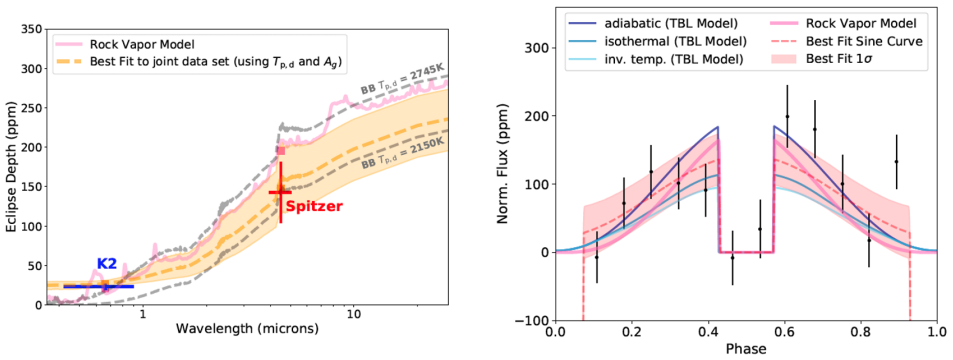

Figure 4: Figure from Zieba et al. (2022). The left panel shows the eclipse depths measured in *Kepler* and *Spitzer* band-passes compared to different emission spectra of the planet. The right panel shows the *Spitzer* phase curve, its best-fit sine curve, and four theoretical phase curves from different models.

Based on the phase curve observation from *Spitzer*, K2-141 b is the first lava planet with an observed phase variation and secondary eclipse at infrared and optical wavelengths, which allows further constraints to be placed on its atmospheric properties (Zieba et al. 2022). The thermal emission of the planet was detected at 3.7σ confidence with an eclipse depth of $f_p/f_* = 141.6^{39.1}_{38.3}$ ppm. K2 and *Spitzer* datasets, in comparison with various toy and physically-motivated models,

indicate a thin rocky vapor atmosphere as the most suitable candidate. A toy model comparison found a non-zero geometric albedo of $A_g = 0.282^{0.070}_{-0.078}$, a dayside temperature of $T_{p,d} = 2049^{362}_{-359}$ K, and a nightside temperature of $T_{p,n} = 956^{489}_{556}$ K (< 1712 K at 2σ) (Kreidberg & Loeb 2016). The high albedo might be caused by a reflective surface or a thermal inversion in the rocky vapor atmosphere (see Section 3.3). Furthermore, a hotspot offset was not evident via observation, which implies a high mean molecular weight or the absence of an atmosphere. When comparing the data to physically motivated models (including a pseudo-2D rock vapor atmosphere model and a 1D Turbulent Boundary Layer (TBL) model), however, both models agree well with the detected phase curve (Castan & Menou 2011, Nguyen et al. 2020, Zieba et al. 2022).

5 Conclusion

In summary, lava worlds are extremely complex environments. The composition, homogeneity, and stability of magma oceans depend on many factors, influencing their ability to probe the interiors within. The magma oceans in turn affect the thermal and chemical properties of the atmospheres, and by extension the observability of lava worlds. Successful observations of lava worlds, primarily using the transit method, are becoming more feasible with existing and future instruments. A small number of examples have been observed and studied in detail, with observations being compared to interior and atmospheric models.

Future observations can provide more insights into the atmospheres and interiors of lava worlds, especially thanks to the recently launched James Webb Space Telescope (JWST). JWST carries instruments with high sensitivity and a sizeable spectroscopic range, and is ideal for studying the thermal emission from highly irradiated lava planets. During the Cycle 1 General Observers program, JWST is scheduled to observe several small USP planets, including the previously mentioned 55 Cnc e and K2-141b (Brandeker et al. 2021, Dang et al. 2021, Espinoza et al. 2021, Hu et al. 2021). These planets' atmospheres might consist of detectable Na, SiO, or SiO_2 caused by the evaporation of their surfaces, which results in broad features at different wavelengths within the JWST MIRI/LRS band-pass (Ito et al. 2015). The MIRI/LRS instrument aboard JWST has a large wavelength coverage ($\sim$5 to $\sim$12 μm), and it is suited for probing the SiO band in determining the presence of an extended atmosphere. The upcoming observations of 55 Cnc e and K2-141 b would provide additional information regarding their atmospheric structures and compositions. New observations could also provide further parameter constraints for future efforts to model lava world atmospheres and interiors, perhaps using codes like `LavAtmos`.

References

Angelo, I., & Hu, R. 2017, AJ, 154, 232, doi: 10.3847/1538-3881/aa9278

Baraffe, I., Chabrier, G., Barman, T. S., et al. 2005, A&A, 436, L47, doi: 10.1051/0004-6361:200500123

Barragán, O., Gandolfi, D., Dai, F., et al. 2018, A&A, 612, A95, doi: 10.1051/0004-6361/201732217

Batalha, N. M., Borucki, W. J., Bryson, S. T., et al. 2011, ApJ, 729, 27, doi: 10.1088/0004-637X/729/1/27

Berger, T. A., Huber, D., van Saders, J. L., et al. 2020, AJ, 159, 280, doi: 10.3847/1538-3881/159/6/280

Borucki, W. J., Koch, D. G., Basri, G., et al. 2011, ApJ, 728, 117, doi: 10.1088/0004-637X/728/2/117

Boukaré, C.-É ., Cowan, N. B., & Badro, J. 2022, The Astrophysical Journal, 936, 148, doi: 10.3847/1538-4357/ac8792

Brandeker, A., Alibert, Y., Bourrier, V., et al. 2021, Is it raining lava in the evening on 55 Cancri e?, JWST Proposal. Cycle 1, ID. #2084

Castan, T., & Menou, K. 2011, The Astrophysical Journal Letters, 743, L36, doi: 10.1088/2041-8205/743/2/L36

Chao, K.-H., deGraffenried, R., Lach, M., et al. 2021, Geochemistry, 81, 125735, doi: 10.1016/j.chemer.2020.125735

Ciardi, D. R., Bean, J., Burt, J., et al. 2019, arXiv e-prints, arXiv:1903.05665, doi: 10.48550/arXiv.1903.05665

Crossfield, I. J. M., Petigura, E., Schlieder, J. E., et al. 2015, ApJ, 804, 10, doi: 10.1088/0004-637X/804/1/10

Dang, L., Cowan, N. B., Hammond, M., et al. 2021, A Hell of a Phase Curve: Mapping the Surface and Atmosphere of a Lava Planet K2-141b, JWST Proposal. Cycle 1, ID. #2347

Dauphas, N., & Chaussidon, M. 2011, Annual Review of Earth and Planetary Sciences, 39, 351, doi: 10.1146/annurev-earth-040610-133428

Deeg, H. J., & Alonso, R. 2018, in Handbook of Exoplanets, ed. H. J. Deeg & J. A. Belmonte (Springer), 117, doi: 10.1007/978-3-319-55333-7_117

Demory, B.-O., Gillon, M., Madhusudhan, N., & Queloz, D. 2016a, MNRAS, 455, 2018, doi: 10.1093/mnras/stv2239

Demory, B.-O., Gillon, M., de Wit, J., et al. 2016b, Nature, 532, 207, doi: 10.1038/nature17169

Dittmann, J. A., Irwin, J. M., Charbonneau, D., et al. 2017, Nature, 544, 333, doi: 10.1038/nature22055

Dorn, C., Hinkel, N. R., & Venturini, J. 2017, A&A, 597, A38, doi: 10.1051/0004-6361/201628749

Dorn, C., & Lichtenberg, T. 2021, The Astrophysical Journal Letters, 922, L4, doi: 10.3847/2041-8213/ac33af

Driscoll, P., & Barnes, R. 2015, Astrobiology, 15, 739, doi: 10.1089/ast.2015.1325

Elkins-Tanton, L. T. 2012, Annual Review of Earth and Planetary Sciences, 40, 113, doi: 10.1146/annurev-earth-042711-105503

Espinoza, N., Bello-Arufe, A., Buchhave, L. A., et al. 2021, The first near-infrared spectroscopic phase-curve of a super-Earth, JWST Proposal. Cycle 1, ID. #2159

Fegley, B., & Cameron, A. G. W. 1987, Earth and Planetary Science Letters, 82, 207, doi: 10.1016/0012-821X(87)90196-8

Garhart, E., Deming, D., Mandell, A., et al. 2020, AJ, 159, 137, doi: 10.3847/1538-3881/ab6cff

Henning, W. G., Renaud, J. P., Saxena, P., et al. 2018, Highly Volcanic Exoplanets, Lava Worlds, and Magma Ocean Worlds: An Emerging Class of Dynamic Exoplanets of Significant Scientific Priority. https://arxiv.org/abs/1804.05110

Howell, S. B., Sobeck, C., Haas, M., et al. 2014, PASP, 126, 398, doi: 10.1086/676406

Hu, R., Demory, B.-O., Seager, S., Lewis, N., & Showman, A. P. 2015, ApJ, 802, 51, doi: 10.1088/0004-637X/802/1/51

Hu, R., Brandeker, A., Damiano, M., et al. 2021, Determining the Atmospheric Composition of the Super-Earth 55 Cancri e, JWST Proposal. Cycle 1, ID. #1952

Ito, Y., Ikoma, M., Kawahara, H., et al. 2015, The Astrophysical Journal, 801, 144, doi: 10.1088/0004-637X/801/2/144

Jehin, E., Gillon, M., Lederer, S. M., et al. 2016, in AAS/Division for Planetary Sciences Meeting Abstracts, Vol. 48, AAS/Division for Planetary Sciences Meeting Abstracts #48, 302.07

Kaltenegger, L., & Traub, W. A. 2009, ApJ, 698, 519, doi: 10.1088/0004-637X/698/1/519

Kite, E. S., Jr., B. F., Schaefer, L., & Gaidos, E. 2016, The Astrophysical Journal, 828, 80, doi: 10.3847/0004-637X/828/2/80

Koch, D. G., Borucki, W. J., Basri, G., et al. 2010, ApJ, 713, L79, doi: 10.1088/2041-8205/713/2/L79

Koll, D. D. B., & Abbot, D. S. 2015, ApJ, 802, 21, doi: 10.1088/0004-637X/802/1/21

Koll, D. D. B., Malik, M., Mansfield, M., et al. 2019, ApJ, 886, 140, doi: 10.3847/1538-4357/ab4c91

Kreidberg, L. 2018, in Handbook of Exoplanets, ed. H. J. Deeg & J. A. Belmonte (Springer), 100, doi: 10.1007/978-3-319-55333-7_100

Kreidberg, L., & Loeb, A. 2016, ApJ, 832, L12, doi: 10.3847/2041-8205/832/1/L12

Léger, A., Grasset, O., Fegley, B., et al. 2011, Icarus, 213, 1, doi: 10.1016/j.icarus.2011.02.004

Leitzinger, M., Odert, P., Kulikov, Y. N., et al. 2011, Planet. Space Sci., 59, 1472, doi: 10.1016/j.pss.2011.06.003

Lopez, E. D. 2017, MNRAS, 472, 245, doi: 10.1093/mnras/stx1558

MacDonald, R. J., Goyal, J. M., & Lewis, N. K. 2020, ApJ, 893, L43, doi: 10.3847/2041-8213/ab8238

Malavolta, L., Mayo, A. W., Louden, T., et al. 2018, AJ, 155, 107, doi: 10.3847/1538-3881/aaa5b5

Malik, M., Kitzmann, D., Mendonça, J. M., et al. 2019, The Astronomical Journal, 157, 170, doi: 10.3847/1538-3881/ab1084

Malik, M., Grosheintz, L., Mendonça, J. M., et al. 2017, The Astronomical Journal, 153, 56, doi: 10.3847/1538-3881/153/2/56

Miguel, Y., Kaltenegger, L., Fegley, B., & Schaefer, L. 2011, The Astrophysical Journal Letters, 742, L19, doi: 10.1088/2041-8205/742/2/L19

Nguyen, T. G., Cowan, N. B., Banerjee, A., & Moores, J. E. 2020, MNRAS, 499, 4605, doi: 10.1093/mnras/staa2487

Parmentier, V., & Crossfield, I. J. M. 2018, in Handbook of Exoplanets, ed. H. J. Deeg & J. A. Belmonte (Springer), 116, doi: 10.1007/978-3-319-55333-7_116

Rauscher, E., Suri, V., & Cowan, N. B. 2018, AJ, 156, 235, doi: 10.3847/1538-3881/aae57f

Ricker, G. R., Winn, J. N., Vanderspek, R., et al. 2014, in Society of Photo-Optical Instrumentation Engineers (SPIE) Conference Series, Vol. 9143, Space Telescopes and Instrumentation 2014: Optical, Infrared, and Millimeter Wave, ed. J. Oschmann, Jacobus M., M. Clampin, G. G. Fazio, & H. A. MacEwen, 914320, doi: 10.1117/12.2063489

Sanchis-Ojeda, R., Rappaport, S., Winn, J. N., et al. 2013, ApJ, 774, 54, doi: 10.1088/0004-637X/774/1/54

Schaefer, L., & Fegley, B. 2004, Icarus, 169, 216, doi: 10.1016/j.icarus.2003.08.023

—. 2009, ApJ, 703, L113, doi: 10.1088/0004-637X/703/2/L113

Schaefer, L., Lodders, K., & Fegley, B. 2012, ApJ, 755, 41, doi: 10.1088/0004-637X/755/1/41

Spencer, J. R., & Schneider, N. M. 1996, Annual Review of Earth and Planetary Sciences, 24, 125, doi: 10.1146/annurev.earth.24.1.125

Stevenson, D. 2010, Treatise on Geophysics, Volume 9: Evolution of the Earth (Elsevier Science). https://books.google.nl/books?id=aYDNCgAAQBAJ

Stock, J. W., Kitzmann, D., Patzer, A. B. C., & Sedlmayr, E. 2018, Monthly Notices of the Royal Astronomical Society, 479, 865, doi: 10.1093/mnras/sty1531

Valencia, D., Sasselov, D. D., & O'Connell, R. J. 2007, The Astrophysical Journal, 665, 1413, doi: 10.1086/519554

Van Buchem, C., Miguel, Y., Zilinskas, M., & van Westrenen, W. 2022, arXiv e-prints, arXiv:2210.10463, doi: 10.48550/arXiv.2210.10463

Zhang, X., & Showman, A. P. 2017, ApJ, 836, 73, doi: 10.3847/1538-4357/836/1/73

Zieba, S., Zilinskas, M., Kreidberg, L., et al. 2022, A&A, 664, A79, doi: 10.1051/0004-6361/202142912

Zilinskas, M., Miguel, Y., van Buchem, C. P. A., & Snellen, I. A. G. 2023, A&A, 671, A138, doi: 10.1051/0004-6361/202245521

Zilinskas, M., van Buchem, C. P. A., Miguel, Y., et al. 2022, A&A, 661, A126, doi: 10.1051/0004-6361/202142984